Chapter 5: Numerical Simulation of Atmospheric Vortex Engine

5.1 Introduction:

The atmospheric vortex engine (AVE) is a green carbon free technology to produce electricity developed by Louis Michaud (http://vortexengine.ca). It uses an artificially created vortex to capture the mechanical energy produced during upward heat convection. The vortex is created by admitting warm or humid air tangentially into the base of a circular wall. The heat source can be solar energy, warm seawater or waste industrial heat. The mechanical energy is produced in peripheral turbo-generators.

The AVE has the same thermodynamic basis as the solar chimney (Schlaich et.al, 2005, Haaf et.al, 1983 and Haaf, 1984). A solar chimney consists of a tall vertical tube, a transparent solar collector surrounding the base and a turbine located at the inlet of the tube. One of the factors influencing the heat to work conversion efficiency of a solar chimney is the height of the chimney. The efficiency is directly proportional to the height. For example the Manzanares solar chimney built in Spain in the 1980's with a 200m tall chimney, diameter of 10 m and solar collector of diameter 250m had a heat to work conversion efficiency of 0.2% and the proposed EnviroMission chimney in Australia has a 1000m tall chimney with a diameter of 130 m and a solar collector of area 40 km^2 has a heat to work conversion efficiency of 3%. The costs of building high chimneys limit their height and in turn their efficiency.

Michaud (1975, 1977) suggested a possible way of eliminating the chimney by imitating naturally occurring tornado-like flows based on the observation that in tornado like vortex flows the convergence is limited to the bottom of the vortex close to the ground and the centrifugal force associated with the circular-velocity limits the convergence (i.e. mixing of ambient air) at other heights. In other words the centrifugal force in a vortex acts as the physical wall of a chimney. This typical convergence characteristic can be easily demonstrated in the case of a laboratory scale numerically simulated tornado. Figure 5.1 illustrates the results from such a study; it shows the

normalized radial and tangential velocity at the core radius along the height. It can be seen that the radial velocity is high close to the ground and reduces along the height whereas the tangential velocity increases along the height and reaches a constant value. The AVE uses the above characteristics of tornadic flow and the physical wall of a chimney is replaced by the centrifugal force of an artificially generated vortex, so the efficiency is not limited by the physical height of the chimney. Also power generation cost is lowered by saving the construction cost of the chimney. Further detailed thermodynamic basis for the AVE are presented in Michaud (1977), Michaud (1995) and Michaud (1996).

In the current chapter numerical simulations of a prototype model-scale AVE are presented. The objective of the simulations is to study the overall flow field produced by the AVE. The effects of varying the geometric and physical parameters are also studied with a view to future design optimization. Further, the effect of cross wind flow is also studied, on a full-scale AVE.

5.2 Numerical simulation:

The prototype model scale AVE has an octagonal column with 8 tangential inlets for the air. The base of the AVE is heated and maintained at a constant temperature. At the roof of the AVE there is a circular opening through which air leaves the AVE and enters the atmosphere. Figures 5.2a and 5.2b show the elevation and plan view of the prototype AVE. The dimensions used in the current simulations for the model-scale geometry are given in Table 5.1. The full-scale geometry is 20 times the model scale and the dimensions are given in Table 5.2.

The computational domain for the simulation is shown in Figure 5.3. It consists of an outer cubic domain 3m X 3m X 2m representing the ambient atmosphere and the AVE is modeled at the centre of the base of the outer cubic domain. The height of the domain chosen is five times the height of the AVE. This is adequate for the preliminary simulations performed here to test effectiveness of the AVE to generate tornado-like

vortex extending beyond its physical height. The side faces of the outer cubic domain are set as inlet boundary conditions with atmospheric pressure and ambient temperature and the top face is set as outlet with atmospheric pressure and ambient temperature. The bottom face is set as wall. The base wall of the AVE is maintained at a constant temperature as a heated plate and the air enters the AVE through the tangential inlet at a higher temperature than the ambient atmosphere. The detailed boundary conditions used in the simulation are given in Table 5.3.

The commercial Computational Fluid Dynamic software, Fluent6.3 was used for the 3D numerical simulation. The software uses Finite Volume Method (FVM) to discretize the equations of motion (Navier-Stokes equations, the continuity equation and the energy equation) and the segregated implicit solver option was employed to solve the equations.

Fluent employs Boussinesq model to solve the buoyancy driven natural convection flow problems. This model assumes density (ρ) as a constant value in all solved equations, except the buoyancy term in the momentum equation. The Boussinesq approximation $\rho = \rho_0(1-\beta\Delta T)$ is used to replace the density from the buoyancy term, where ρ_0 is the constant density, β is the thermal expansion coefficient and $\Delta T = (T - T_0)$ is the temperature difference between actual and ambient temperature (Fluent 6.3, 2006). This model was used in the current AVE simulations. The Boussinesq approximation is only valid when $\beta(T - T_0) << 1$, and in the current simulations $\beta(T - T_0) \approx 0.067$. Details of this value and the other physical parameters of relevance are presented in Appendix C.

In buoyancy driven flows Rayleigh number Ra < 10^8 indicates a buoyancy–induced laminar flow and transition to turbulence occurs over the range of 10^8 < Ra < 10^{10}. In the current simulations Ra = 2.06 X 10^9 for the model-scale AVE. Even though the Rayleigh number for the flow in AVE indicate a transitional turbulence induced buoyancy flow, a pilot study was carried out using laminar simulations on the model-scale AVE to do an initial assessment of the flow field. Further simulations were carried out using the second

order unsteady k-ε turbulence model. An unstructured grid was used and further grid convergence was done and grid sizes were considered to be sufficient to cover the domain in its relevant details. For the model-scale AVE, around 200,000 cells were used for laminar simulations and 400,000 cells were used for turbulent simulations. Around 800,000 cells were used for the full-scale simulations. The interaction of the vortex flow with the base of the AVE was not the focus of the study, so a standard wall function model was used in the near-wall region. The SIMPLEC pressure velocity coupling and second order discretization for pressure, momentum, energy, turbulent kinetic energy and specific dissipation rate were employed.

5.2.1 Preliminary laminar simulations on model-scale AVE:

A preliminary laminar simulation was performed for a temperature difference of $\Delta T = 20$ K between the inlet air and ambient air. Figures 5.4 and 5.5 show the contour plot of the tangential velocity in the YZ plane and the vector plot of velocity magnitude at Z =0.4m plane (at the exit of AVE). It can be seen from these plots that a tornado like vortex flow was generated inside the AVE and the flow extended into the atmosphere till the top of the domain. Figure 5.6 shows the contour plot of temperature in the YZ plane. It can be seen that the warm plume does not get dissipated and the high temperature is maintained till the top of the domain, confirming the earlier statement that the vortex acts like a physical chimney and arrests the dissipation of heat at heights above the AVE. Figure 5.7 shows the contour plot of the velocity magnitude in the YZ plane. It shows the two-celled structure characteristic of high swirl ratio tornadic flows. The maximum velocity of 1.15 m/s was obtained near the top of the domain and the velocity of the air as it exits the vortex generator was around 0.687 m/s. Figure 5.8 shows the contour plot of static pressure in the YZ plane and the pressure drop in the region around the center is also characteristic of the tornadic flow as discussed in section 2.2.4.

All these observations namely, tangential velocity, temperature, velocity magnitude and static pressure taken together signify that the AVE is able to generate a tornado-like vortex flow sustaining the high temperature till the top of the domain.

5.2.2 *k-ε* simulations on model-scale AVE:

The above simulation was performed again using *k-ε* turbulence model for the same temperature difference of $\Delta T = 20$ K between the inlet air and ambient air. Figures 5.9 and 5.10 show the contour plot of the tangential velocity and velocity magnitude in the YZ plane respectively. These figures again confirm that the AVE produces vortex like flow and it extends into the atmosphere. The maximum velocity magnitude and the tangential velocity of the turbulent simulations are smaller than the laminar case because of the energy dispersion due to turbulence.

5.2.3 Design optimization:

The CFD simulations indicate that the current model-scale AVE geometry can produce a spiraling upward flow extending well above the AVE. The current dimensions of the key geometric parameters like deflector gap 'g1' (5% of deflector diameter ring 'd1'), tangential entry height 'h1' (20% of deflector diameter ring 'd1'), octagonal cylinder height 'h2' (20% of deflector diameter ring 'd1'), roof opening 'D3' (30% of deflector diameter ring 'd1') have produced satisfactory results and is a good starting point for future designs. Further design optimization of AVE can be achieved by studying the effects of changes in physical and geometric parameters in the model-scale AVE. The changes in geometric parameters like increased roof opening (D3), and increased domain height (Z), and changes in physical parameters like increased temperature difference between inlet air and ambient temperature (ΔT) were studied here. Both laminar and turbulent *k-ε* simulations were performed for all the three cases.

The contour plot of static pressure (Figure 5.8) shows that there is build up of pressure near the roof of the AVE. To reduce the area of the roof, the roof opening (D3) diameter was increased from 300mm to 600mm. The increase in roof opening did not affect the vortex other than causing an increase on the diameter of vortex formed. Figure 5.11 shows the contour plot velocity magnitude of the vortex in the YZ plane for the

increased roof opening. It was inferred that the roof opening diameter is not a critical parameter and future designs should adopt the smaller diameter (30% of deflector diameter ring 'd1') to produce a tight vortex and avoid the straight octagonal cylinder with roof by replacing it with a convergent octagonal cylinder.

The vertical domain height was increased from 2000 mm to 6000 mm. Figures 5.12 and 5.13 show the contour plot velocity magnitude and temperature of the vortex in the YZ plane for the extended domain. The increase in the height does not dissipate the temperature much and plume extends till the top of the domain.

The key physical parameter, temperature difference between the inlet air and ambient air (ΔT) was increased from 20 K to 30 K. The increase produced a much stronger vortex. Figure 5.14 shows the contour plot of velocity magnitude of the vortex in the YZ plane for ΔT = 30 K case and the maximum velocity is approximately 20% higher than the ΔT = 20 K case (Figure 5.9). It can be concluded that for a given geometric configuration of AVE, the vortex strength and in turn the power output is mainly controlled by temperature difference between the inlet air and ambient air (ΔT).

5.2.4 Full-scale AVE simulations with cross wind:

The results presented so far pertain to a lab scale model which will be studied indoors and atmospheric wind plays no roll in this situation. Full-scale AVE will be located outdoors and will be subject to the influence of atmospheric wind. A full-scale AVE with geometry 20 times the model-scale AVE has been proposed to be built. Simulation of a full-scale AVE was done to study the effect of cross wind on the vortex generated. Detailed domain dimensions used in the simulation are given in Table 5.2. For the full-scale dimensions considered here the Rayleigh number Ra = 1.648×10^{13}. This indicates that the flow will be turbulent in nature, so k-ε turbulent model simulations were performed.

An initial simulation without cross wind was performed as base case for comparison with the cross wind case. Figure 5.15 shows the contour plot velocity magnitude of the vortex in the YZ plane and Figure 5.16 shows the static pressure in the YZ plane. The features observed in these figures are similar to those observed in the model scale simulations, confirming the formation of tornado-like flows in the full-scale AVE also. The simulation was repeated with the inclusion of horizontal cross wind in the positive X direction. The horizontal wind has a power law mean velocity profile corresponding to an open terrain (with a velocity of 1.2 m/s at 10 m height).

Figures 5.17 and 5.18 show the contour plot of velocity and temperature in the XZ plane for the full scale geometry with cross flow of wind. As expected the column of vortex gets tilted in the direction of the wind. The pressure contours shown in Figure 5.19 indicate that even though the plume gets tilted, the changes in pressure drop at the base of the AVE is negligible when compared to that of the no cross wind case (Figure 5.16). The pressure drop at the base of the AVE is responsible for drawing the air inside the AVE and driving the turbo-generators located at the inlets, so even though the cross wind tilts the vortex, it does not greatly affect the power generation capacity of the AVE.

5.3 Conclusion:

The CFD analysis of a model-scale Atmospheric Vortex Engine (AVE) was performed. The results show that the AVE can generate a vortex flow in the atmosphere much above the AVE and the vortex acts as a physical chimney limiting the mixing of surrounding air into the raising plume of hot air. A parametric study was conducted and provides a good starting point for future designs. For a given geometry, the physical parameter ΔT (temperature difference between the inlet air to AVE and ambient air) is the main parameter that controls the strength of the vortex and in turn the power output. The full scale simulations subjected to cross wind show that the power generation capacity is not affected by the cross winds.

The current full scale simulations do not consider actual temperature gradient present in the atmosphere. Future studies should include the effect of various atmospheric stratifications: stable, unstable and neutral for further accurate results.

5.4 References:

Haaf, W., 1984. Solar Chimneys - Part II: Preliminary Test Results from the Manzanares Pilot Plant. International Journal of Solar Energy 2(2), 141–161.

Haaf, W., Friedrich, K., Mayr, G., and Schlaich, J., 1983. Solar Chimneys. Part 1: Principle and Construction of the Pilot Plant in Manzanares. International Journal of Solar Energy 2(1), 3–20.

Fluent 6.3 User's guide, 2006. Fluent Inc, Lebanon, USA.

Michaud, L. M., 1975. Proposal for the use of a controlled tornado-like vortex to capture the mechanical energy produced in the atmosphere from solar energy. Bulletin of the American Meteorological Society 56, 530-534.

Michaud, L. M., 1977. On the energy and control of atmospheric vortices. Journal de Recherches Atmospheriques 11(2), 99-120.

Michaud, L. M., 1995. Heat to work conversion during upward heat convection. Part I: Carnot engine method. Atmospheric Research 39, 157-178.

Michaud, L. M., 1996. Heat to work conversion during upward heat convection. Part II: Internally generated entropy method. Atmospheric Research 41, 93-108.

Michaud, L. M., 1999. Vortex process for capturing mechanical energy during upward heat-convection in the atmosphere. Applied Energy 62, 241-251.

Schlaich, J., Bergermann, R., Schiel, W., and Weinrebe, G., 2005. Design of commercial solar tower systems—utilization of solar induced convective flows for power generation, Journal of Solar Energy Engineering 127, 117-124.

Parameter Name	Parameter Description	Base Value (mm)
d1	Inner octagonal cylinder diameter	1000
d2	Outer octagonal cylinder diameter	1050
d3	Roof opening diameter	300
d4	Floor opening diameter	0
d5	Upper circular cylinder diameter	800
g1	Gap between deflectors	50
h1	Tangential entry height	200
h2	Octagonal cylinder height	200
h3	Upper cylinder height	0
Z	Domain height	2000

Table 5.1: Dimensional specifications for prototype model-scale AVE

Parameter Name	Parameter Description	Base Value (m)
d1	Inner octagonal cylinder diameter	20
d2	Outer octagonal cylinder diameter	21
d3	Roof opening diameter	6
d4	Floor opening diameter	0
d5	Upper circular cylinder diameter	16
g1	Gap between deflectors	1
h1	Tangential entry height	4
h2	Octagonal cylinder height	4
h3	Upper cylinder height	0
Z	Domain height	120

Table 5.2: Dimensional specifications for prototype full-scale AVE

Boundary name	Boundary condition
Cubic domain side wall (4)	Pressure Inlet (Atm Pr, Ambient Temp T)
Cubic domain roof	Pressure outlet (Atm Pr, Ambient Temp T)
Cubic domain base	Free-slip wall
Tangential air inlet (8)	Pressure inlet (Atm Pr, Ambient Temp T + ΔT)
AVE base	No-slip wall (Temp T + ΔT)
AVE roof opening	Interior
AVE deflectors	No-slip wall
AVE octagonal cylindrical wall	No slip wall
AVE roof	No slip wall

Table 5.3: Boundary conditions for both model-scale and full-scale AVE simulations

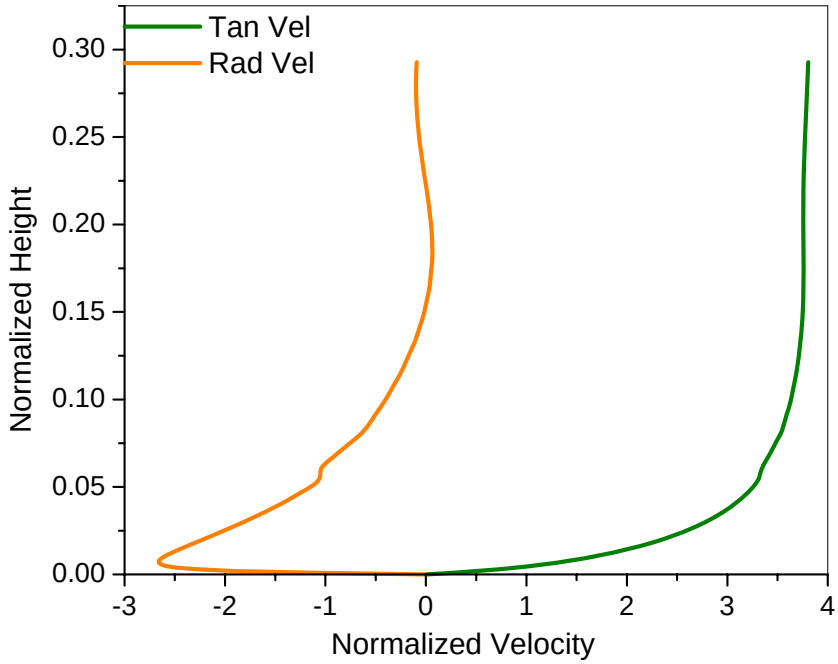

Figure 5.1: The radial and tangential velocity along the height at the core radius of a typical numerically simulated laboratory scale tornado.

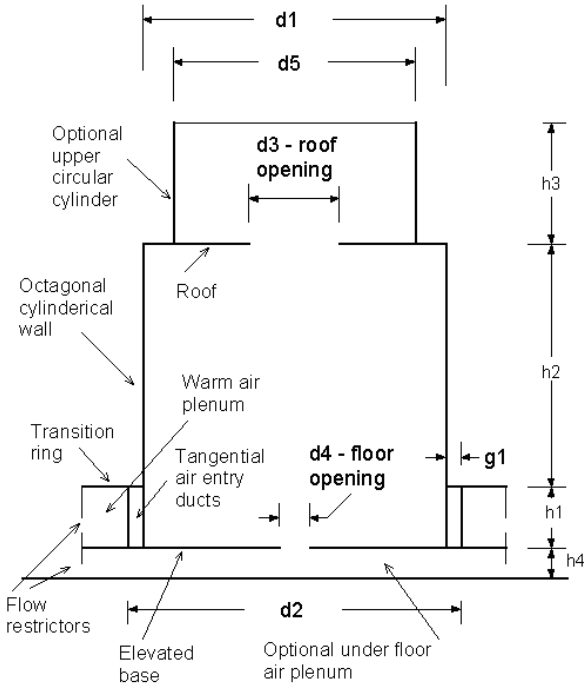

Figure 5.2a: Geometry of the prototype AVE used in the current simulations (Elevation)

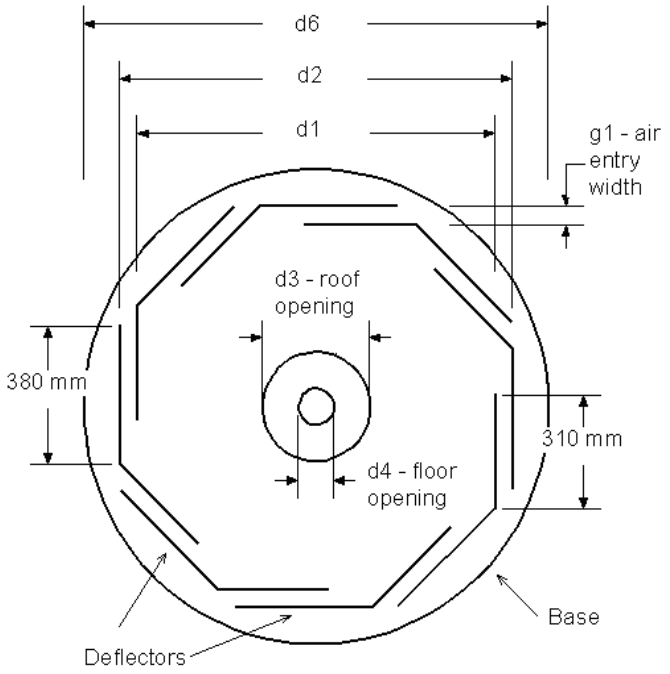

Figure 5.2b: Geometry of the prototype AVE used in the current simulations (Plan view)

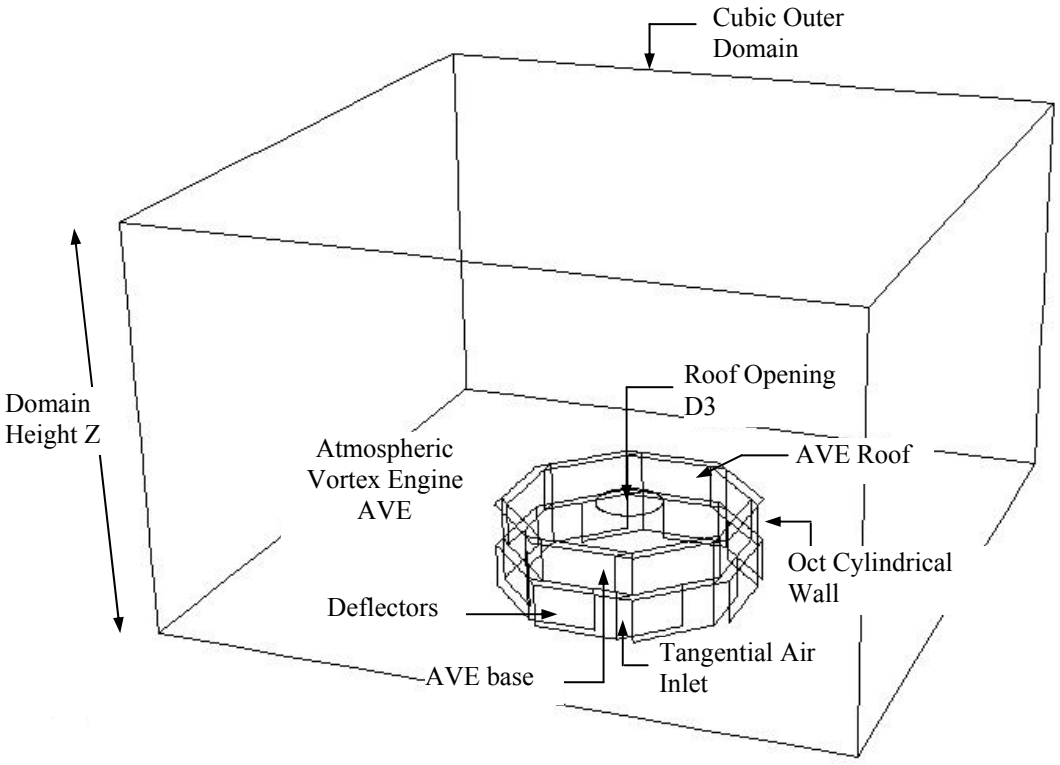

Figure 5.3: The computational domain

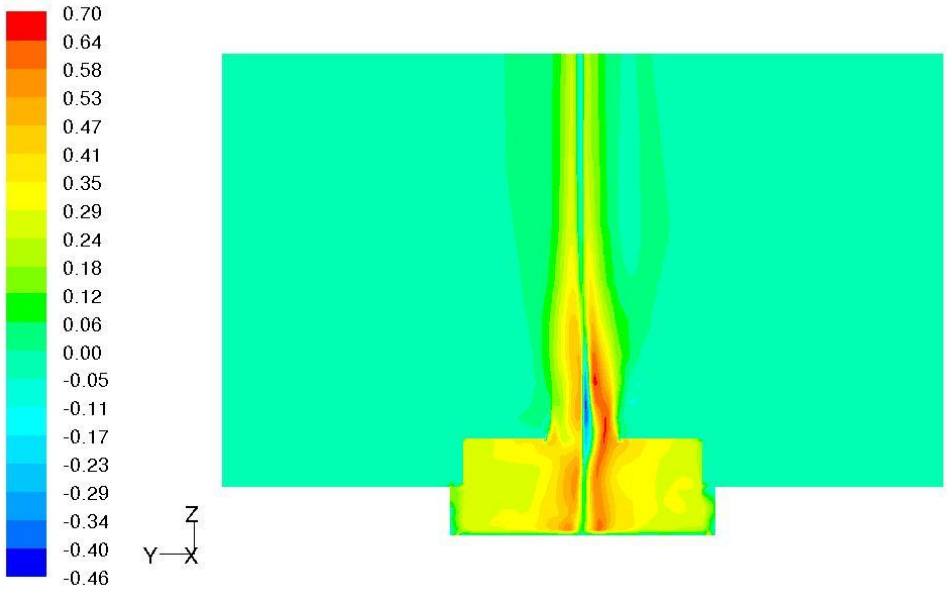

Figure 5.4: The contour plot of tangential velocity (m/s) in the YZ plane for model-scale AVE (Laminar Simulations)

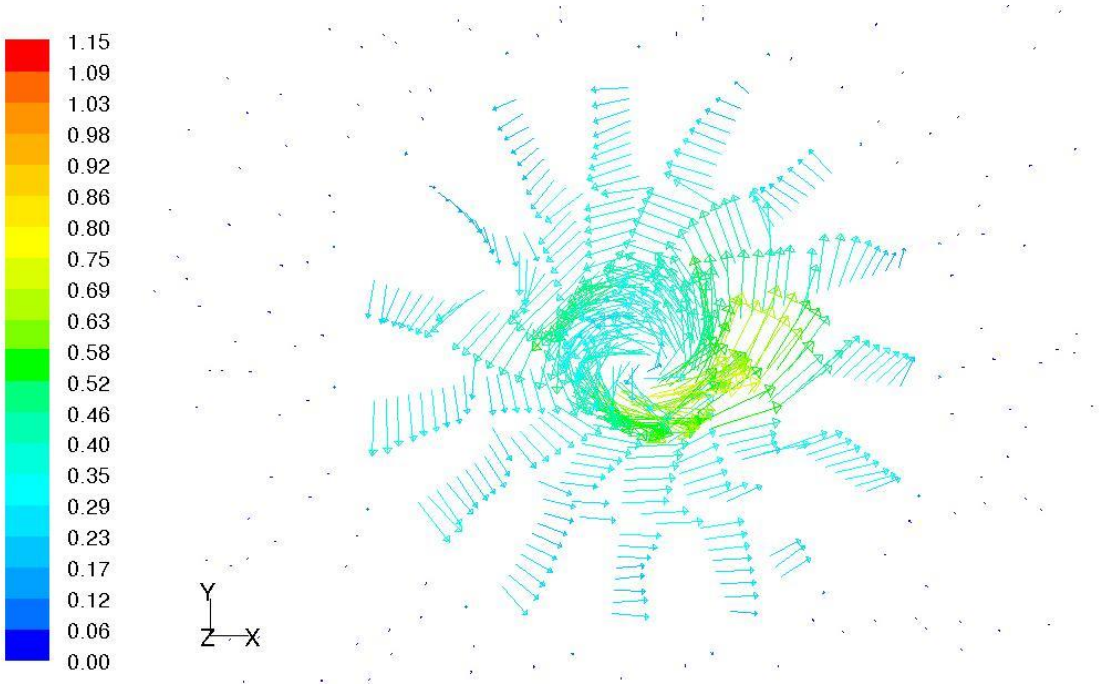

Figure 5.5: The vector plot of velocity magnitude (m/s) in the Z =0.4m plane for model-scale AVE (Laminar Simulations)

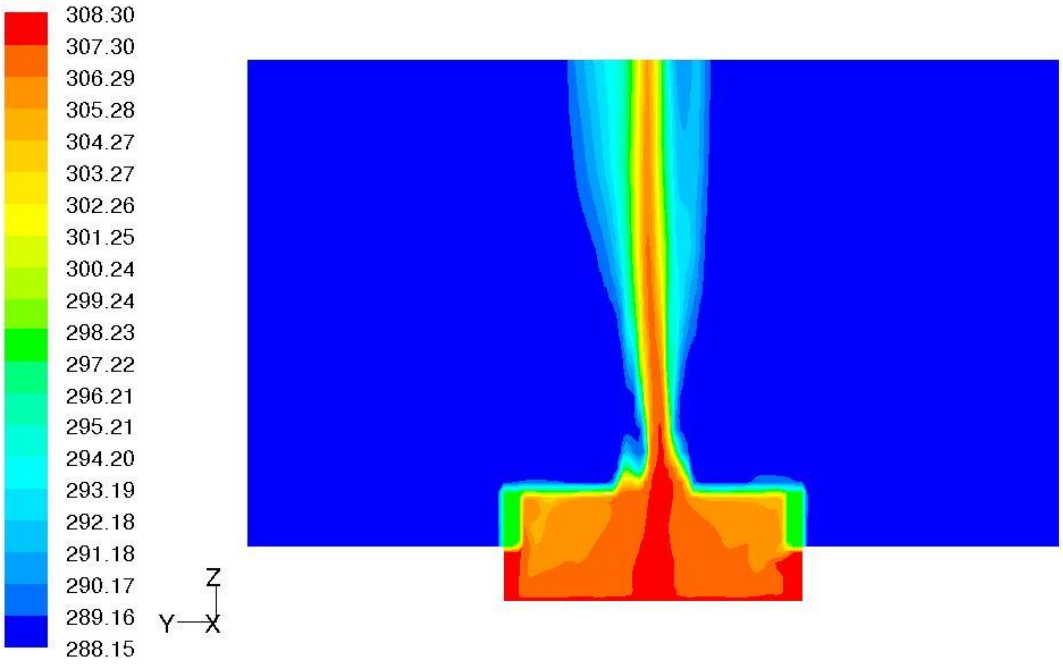

Figure 5.6: The contour plot of temperature (K) in the YZ plane for model-scale AVE (Laminar Simulations)

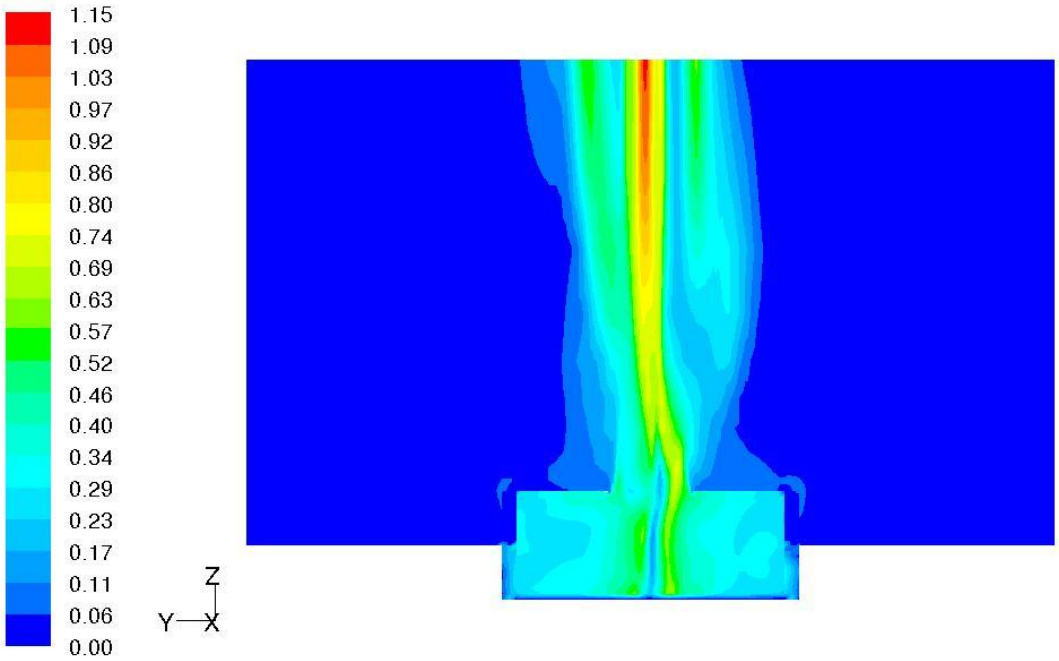

Figure 5.7: The contour plot of velocity magnitude (m/s) in the YZ plane for model-scale AVE (Laminar Simulations)

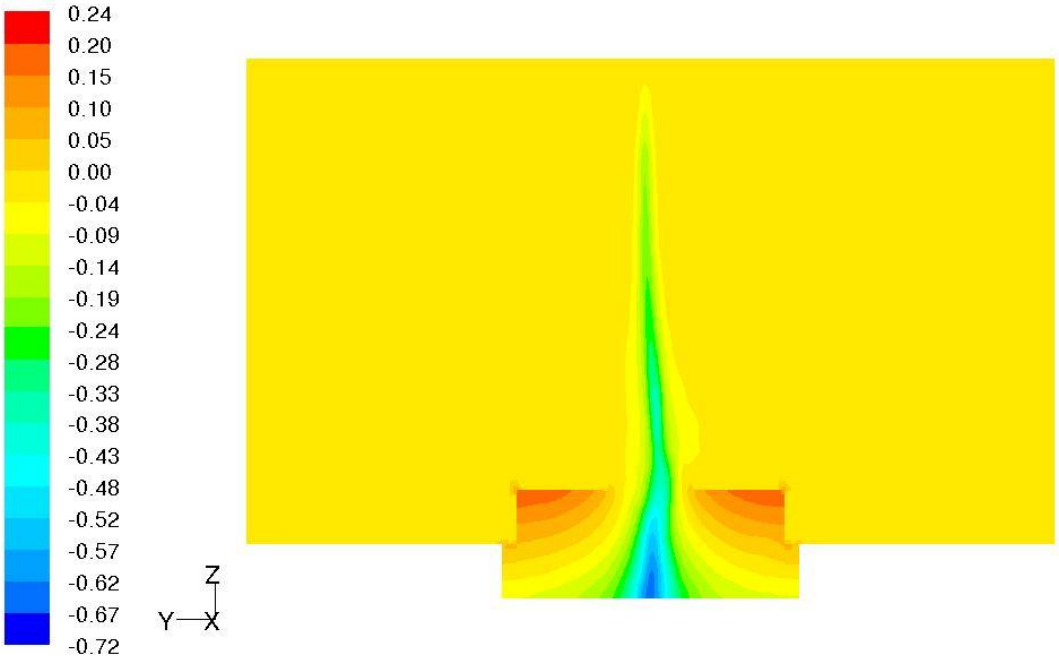

Figure 5.8: The contour plot of static pressure (Pa) in the YZ plane for model-scale AVE (Laminar Simulations)

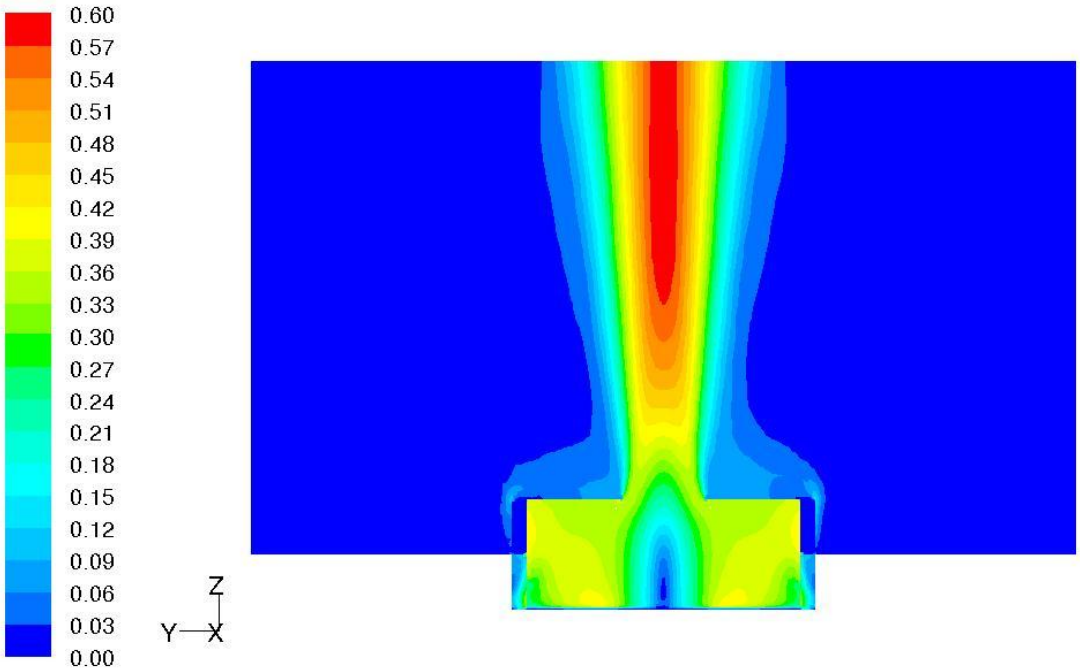

Figure 5.9: The contour plot of velocity magnitude (m/s) in the YZ plane for model-scale AVE (Turbulent Simulations)

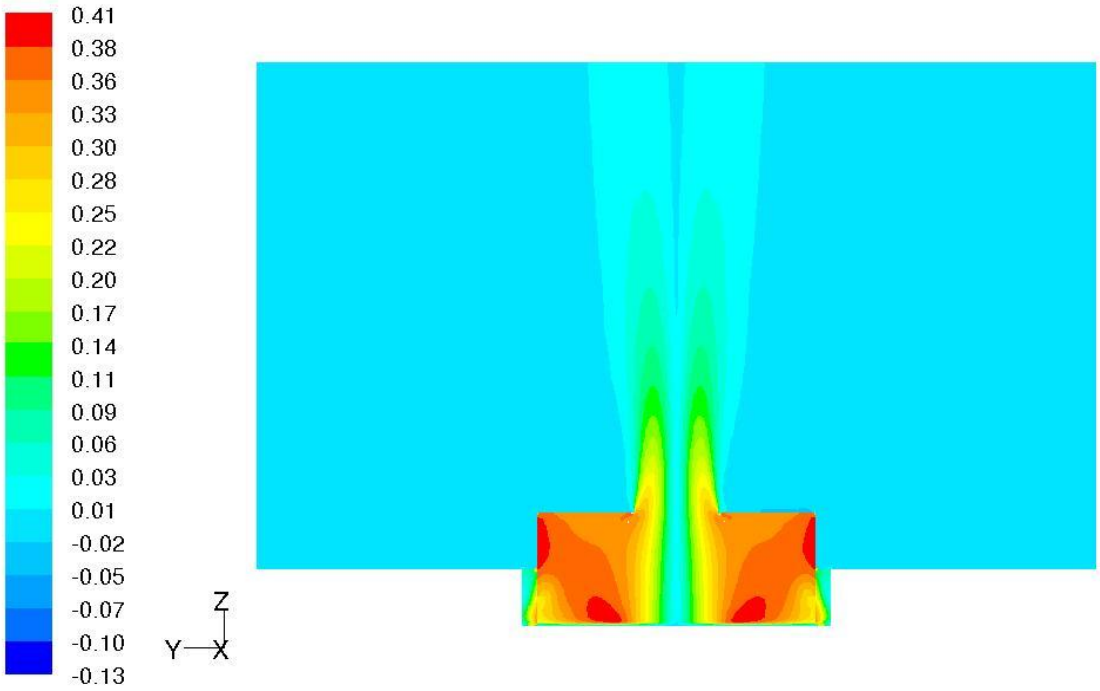

Figure 5.10: The contour plot of tangential velocity (m/s) in the YZ plane for model-scale AVE (Turbulent Simulations)

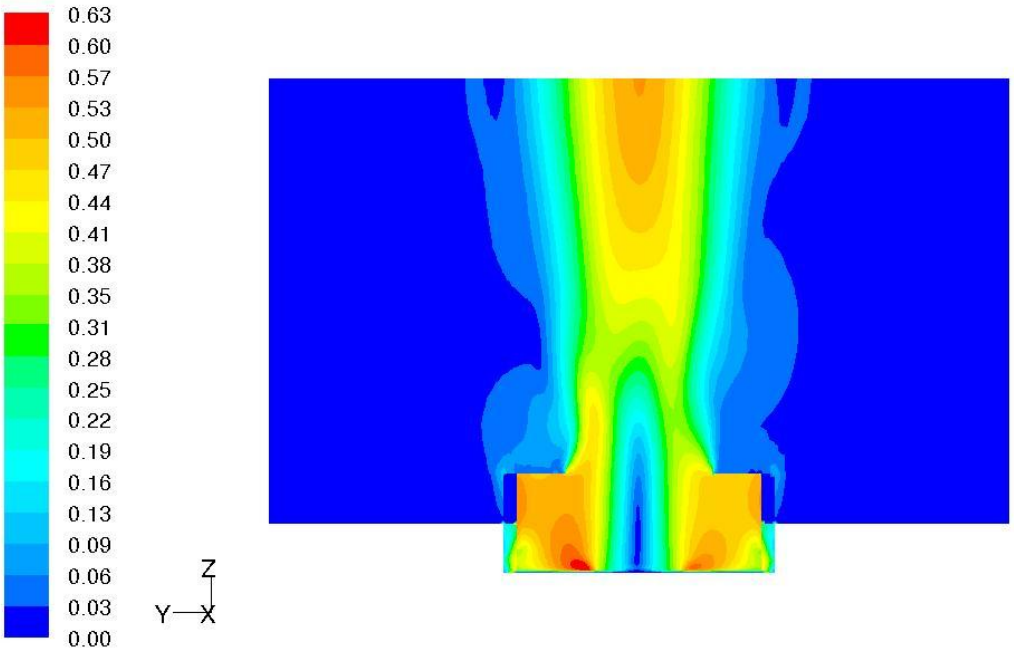

Figure 5.11: The contour plot of velocity magnitude (m/s) in the YZ plane for model-scale AVE with increased roof opening diameter D3 (Turbulent Simulations)

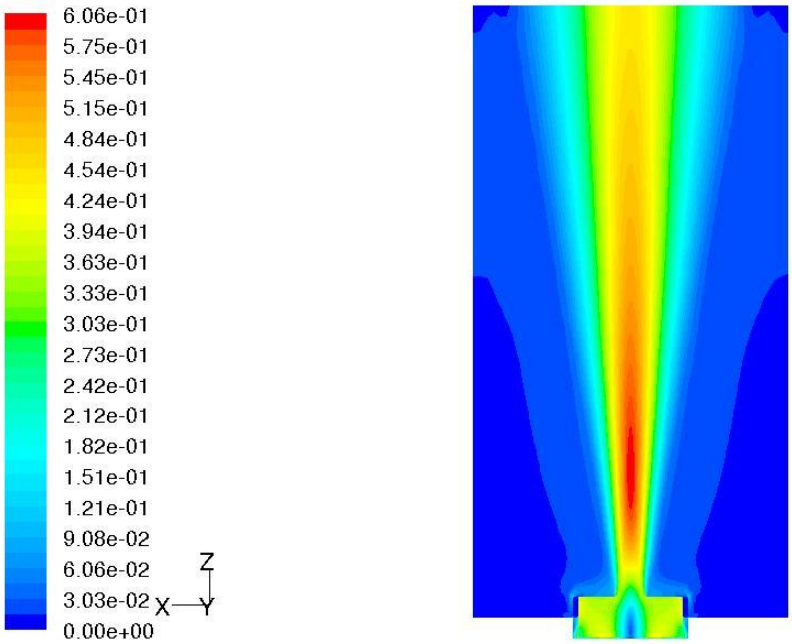

Figure 5.12: The contour plot of velocity magnitude (m/s) in the YZ plane for the extended domain (Z = 6000mm) model-scale AVE (Turbulent Simulations)

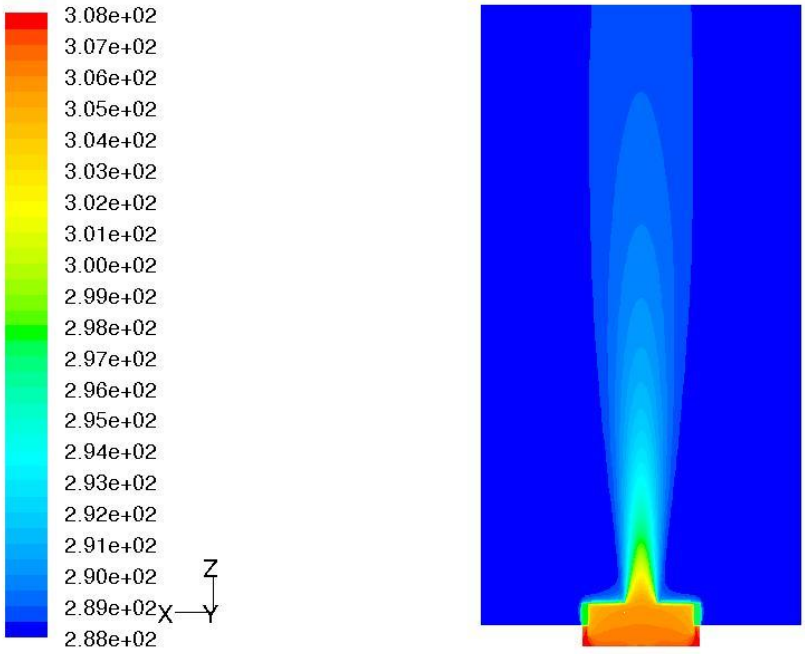

Figure 5.13: The contour plot of temperature (K) in the YZ plane for the extended domain (Z = 6000mm) model-scale AVE (Turbulent Simulations)

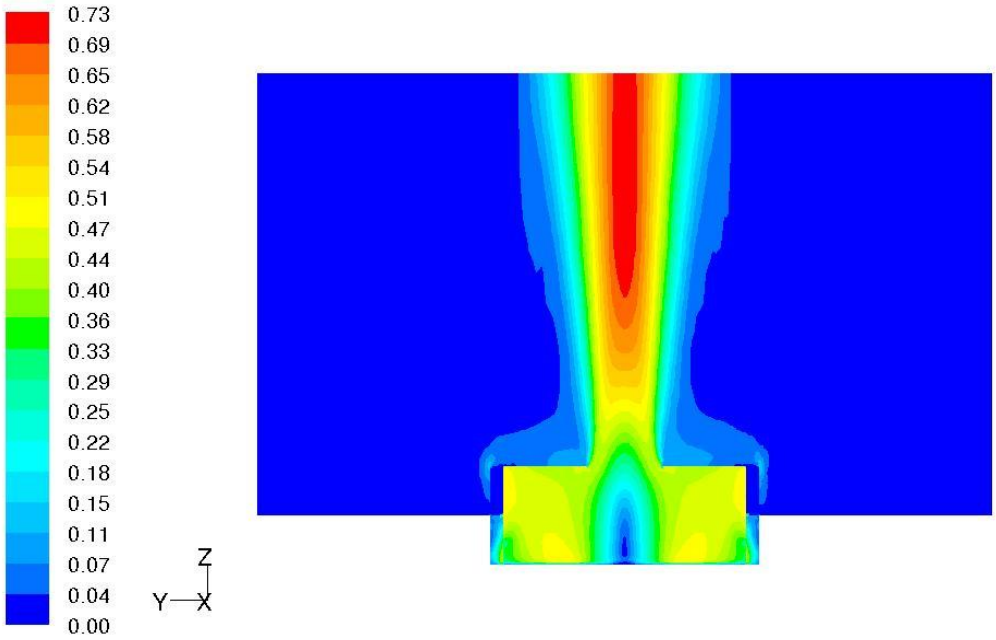

Figure 5.14: The contour plot of velocity magnitude (m/s) in the YZ plane for model-scale AVE with increased temperature difference between the inlet air and ambient air (ΔT = 30 K) (Turbulent Simulations)

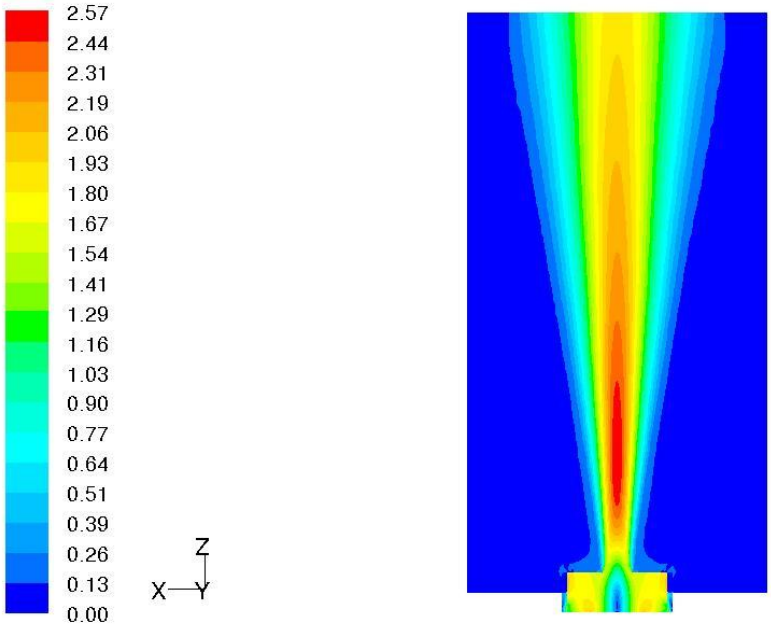

Figure 5.15: The contour plot of velocity magnitude (m/s) in the YZ plane for the full-scale AVE

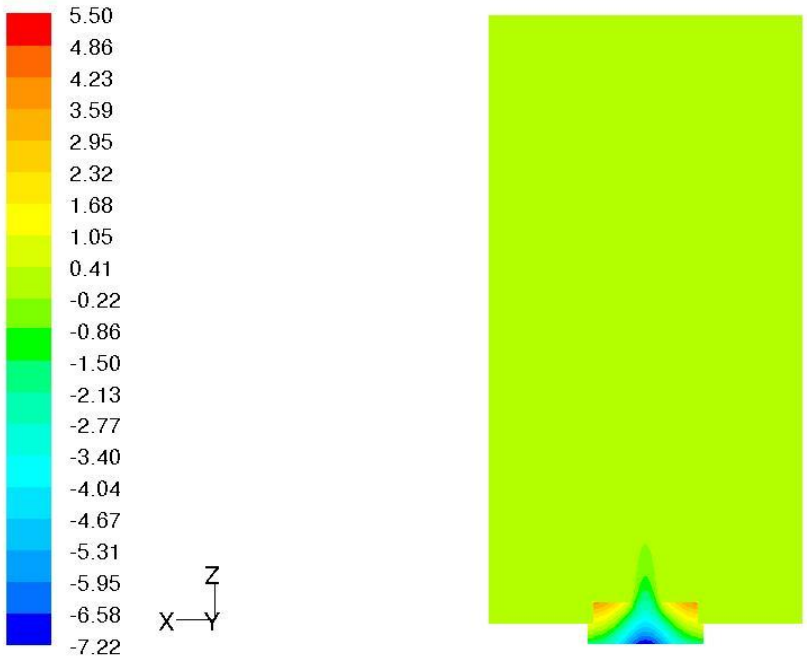

Figure 5.16: The contour plot of static pressure (Pa) in the YZ plane for the full-scale AVE

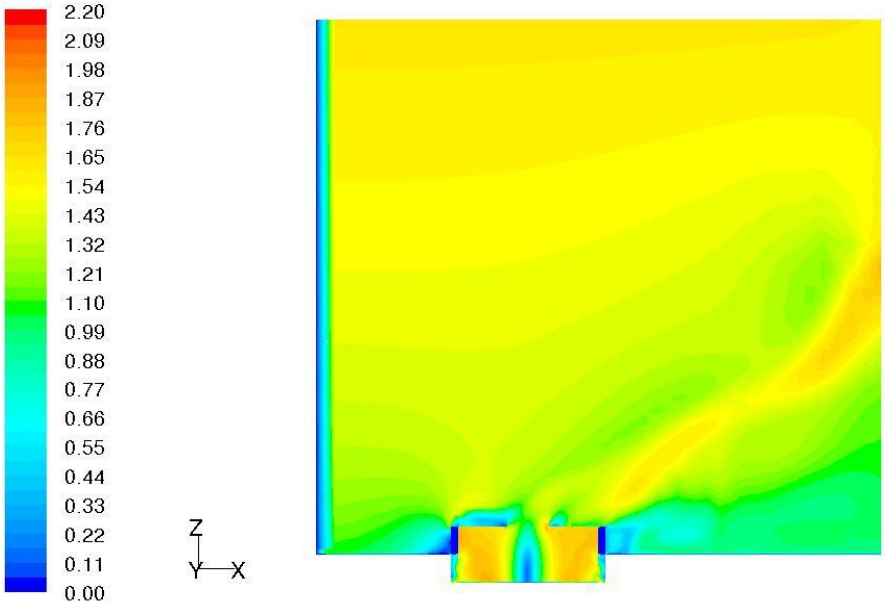

Figure 5.17: The contour plot of velocity magnitude (m/s) in the YZ plane for the full-scale AVE with cross wind

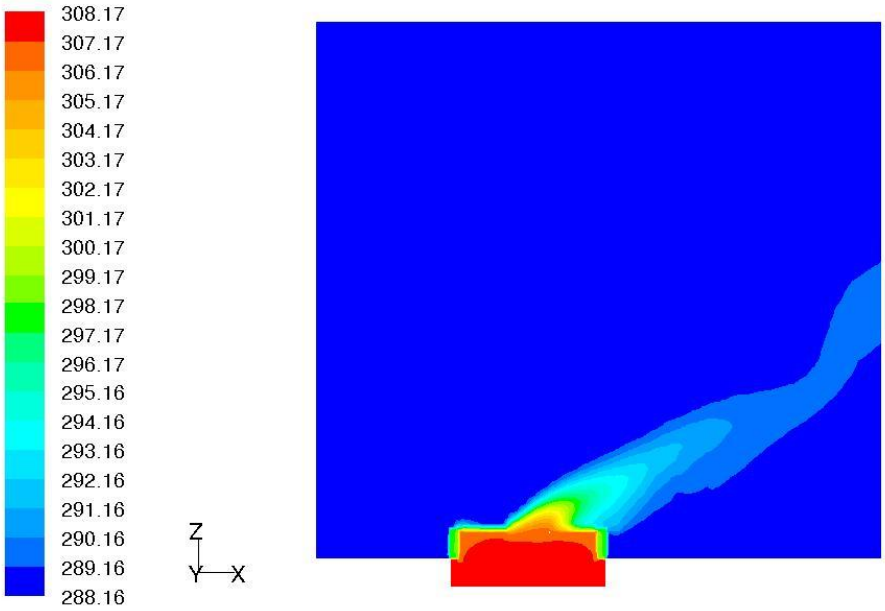

Figure 5.18: The contour plot of temperature (K) in the YZ plane for the full-scale AVE with cross wind

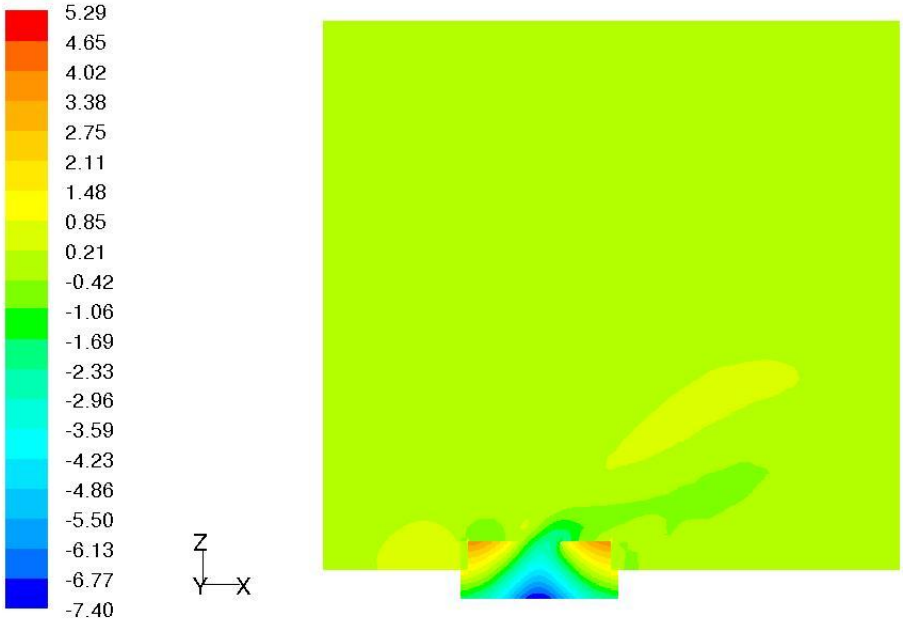

Figure 5.19: The contour plot of static pressure (Pa) in the YZ plane for the full-scale AVE with cross wind

Appendix C: Rayleigh number calculation for AVE simulations

Rayleigh number (Ra):

$$Ra = \frac{g\beta(T_S - T_\infty)x^3}{\nu\alpha}$$

Variables	Model-scale AVE	Full-scale AVE
AVE base diameter: X (m)	1	20
Inlet air temperature: T_S (K)	308.16	308.16
Ambient temperature: T_∞ (K)	288.16	288.16
Film Temp: $T_f = \frac{T_S + T_\infty}{2}$	298.16	298.16
Thermal expansion coefficient (1/K): $\beta = \frac{1}{T_f}$	3.35×10^{-3}	3.35×10^{-3}
Kinematic viscosity at T_f: ν (m^2/s)	1.5×10^{-5}	1.5×10^{-5}
Thermal diffusivity at T_f: α (m^2/s)	2.112×10^{-3}	2.112×10^{-3}
Ra	2.06×10^{9}	1.648×10^{13}

Boussinesq model:

The Boussinesq approximation is only valid when $\beta(T - T_0) << 1$. In the current simulations the temperature difference between actual and ambient temperature $\Delta T = (T - T_0) = (308.16 - 288.16) = 20K$ and the thermal expansion coefficient $\beta = 3.35X10^{-3}$ 1/K, therefore $\beta(T - T_0) = 0.067$.